



CHORUS

This is the accepted manuscript made available via CHORUS. The article has been published as:

Spin-orbit torque from a ferromagnetic metal

Hao Wu, Seyed Armin Razavi, Qiming Shao, Xiang Li, Kin L. Wong, Yuxiang Liu, Gen Yin,
and Kang L. Wang

Phys. Rev. B **99**, 184403 — Published 6 May 2019

DOI: [10.1103/PhysRevB.99.184403](https://doi.org/10.1103/PhysRevB.99.184403)

Spin-orbit torque from a ferromagnetic metal

Hao Wu^{*}, Seyed Armin Razavi, Qiming Shao, Xiang Li, Kin L. Wong, Yuxiang Liu,
Gen Yin, and Kang L. Wang^{*}

*Department of Electrical and Computer Engineering, and Department of Physics and
Astronomy, University of California, Los Angeles, California 90095, United States*

^{*}Corresponding author. E-mail: wuhaophysics@ucla.edu, wang@ee.ucla.edu

Abstract:

The switching of magnetization by current-induced spin-orbit torque (SOT) has potential applications for energy-efficient spintronic devices. In the past, most conventional works have been focused on SOT in heavy metals. Here the SOT from a ferromagnetic metal is investigated, and two mechanisms of the field-free SOT induced magnetization switching are demonstrated to be from the interlayer exchange coupling and the tilted perpendicular magnetic anisotropy. We exclude the spin torque contribution from the anomalous Hall effect and the interfacial Rashba effect combined with spin precession. A spin Hall angle $\theta_{SH} = -0.022$ of CoFeB is obtained by the current-induced hysteresis loop shift method, and the obtained θ_{SH} is comparable with heavy metals. This work demonstrates that a considerable SOT can come from a ferromagnetic metal, and indicates the unconventional origin of SOC.

Main Text:

The electrical manipulation of magnetic moment by spin-orbit torque (SOT) provides an energy efficient method for practical magnetic memory and logic applications [1-3]. Previously SOT induced magnetization switching originates from the spin Hall effect

(SHE) [4-8] in heavy metals has been demonstrated [2, 3], however, in order to realize the deterministic switching, an external magnetic field along the current axis is needed to break the inversion symmetry. Recently, field-free SOT switching has been achieved by the methods of symmetry-breaking of the structure [9], tilted perpendicular magnetic anisotropy [10], interlayer exchange coupling [11], exchange bias effect [12-16], and other methods [17, 18]. In order to improve the energy efficiency, exploring new systems and mechanisms to increase the SOT efficiency has drawn many attentions, such as spin-momentum locking from topological insulators [19] and Rashba-Edelstein effect from the metal oxide/metal interface [20, 21].

Typically, SOT is driven by the spin current injection via SHE in heavy metals with strong spin-orbit coupling (SOC). It is known that besides heavy metals, ferromagnetic metals also possess strong SOC, which leads to magnetoelectric transport properties such as anisotropic magnetoresistance, anomalous and planar Hall effect [22, 23]. Previous works have showed that the inverse spin Hall effect (ISHE) could be observed in NiFe [24, 25] and CoFeB [26], and the extracted spin Hall angle is comparable with heavy metals. Therefore, utilizing the SOT from a ferromagnetic metal provides another method to achieve current-induced magnetization switching [27-30]. Moreover, in ferromagnetic metals, anomalous Hall effect (AHE) [31] which originates from the spin dependent scattering could also contribute to the spin-charge conversion [32].

In this work, we investigate the SOT induced magnetization switching in an exchange-coupled system consisting of an in-plane ferromagnetic layer and another

perpendicular ferromagnetic layer separated by a wedged Mo layer, i.e., I-CoFeB/Mo(wedged)/P-CoFeB, where the I-CoFeB and P-CoFeB layers have the in-plane and perpendicular magnetic anisotropy (IMA and PMA), respectively. We realize the field-free SOT switching using two methods: (i) the interlayer exchange coupling (IEC) when the magnetization of I-CoFeB and current directions are colinear to each other; (ii) the tilted PMA when the magnetization of I-CoFeB and current directions are orthogonal. We find that the SOT comes from the bulk SHE in the I-CoFeB layer in both cases, which cannot be explained by the previous ideas of the anomalous Hall effect and the interfacial Rashba effect combined with spin precession.

The test sample Mo(2)/CoFeB(3)/Mo(2-wedged)/CoFeB(1.1)/MgO(2) and the control sample Mo(2)/CoFeB(1.1)/MgO(2) (thicknesses in nanometers) are deposited on Si-SiO₂ substrates by a magnetron sputtering system, and an 200 °C in-situ annealing is carried out to improve the PMA of the top CoFeB layer. Then the stacks are patterned into Hall-bar devices by the standard photo lithography combined with a dry etching method. The magnetic properties are measured with a vibrating sample magnetometer, and the spin transport properties are measured with a four-probe station with an electromagnet. All measurements are carried out at room temperature.

The 3-dimensional schematic of the test sample is shown in Fig. 1(a), where the top CoFeB layer is designed with PMA, while the bottom CoFeB layer has IMA. The interlayer Mo between the top and bottom CoFeB layers is wedged along the y axis, which induces a small tilt angle of the PMA of the top CoFeB layer from the z axis to

the y axis. The patterned Hall-bar device with the dimension of $20 \times 130 \mu\text{m}^2$ is shown in the bottom figure. The magnetic loops under magnetic fields along x , y , and z axes are shown in Fig. 1(b), which illustrate the PMA of the top CoFeB layer and the IMA of the bottom CoFeB layer. We also observe a small uniaxial anisotropy of the bottom I-CoFeB along the wedged (y) axis with an anisotropy field H_k of 13.5 Oe, which is induced by the IEC between the top tilted P-CoFeB layer and the bottom I-CoFeB layer, and we will discuss the details later.

Next, the SOT induced magnetization switching measurement is conducted for the test sample. As shown in Fig. 2(a), an external magnetic field H_x is applied to align the magnetization of the I-CoFeB layer to the x direction firstly and then a 1-ms writing current pulse I_x is applied along the x direction to provide the SOT to the P-CoFeB layer, for reading another 1-ms current pulse I_R (1 mA) is applied to detect the magnetization of the P-CoFeB layer from the AHE voltage. The spin current with the y -direction spin polarization σ is generated due to the spin Hall effect in the I-CoFeB layer, and then the spin current is injected to the P-CoFeB layer, where the damping-like torque induces the magnetization switching [33, 34]. The inversion symmetry breaking of the up and down magnetization states of the P-CoFeB layer is realized by the x -directional effective field induced by the IEC from the I-CoFeB layer. It should be mentioned that the spin current generated by AHE in the I-CoFeB should satisfy $\mathbf{J}_s \propto \mathbf{J}_e \times \mathbf{M}$, so in this case ($\mathbf{J}_e // \mathbf{M}$) AHE has no contribution to the spin current because of the colinear orientation of the current and the magnetization. From the planar Hall signal in Fig. 2(b), we can obtain the coercivity of the I-CoFeB to be

5.5 Oe. A constant magnetic field varying from +100 Oe to -100 Oe is applied during the SOT switching measurement, as shown in Fig. 2(c), and the key points are discussed below: firstly, the zero-field switching is realized via the IEC from the I-CoFeB layer, and the switching current density at zero field is 1.66×10^7 A/cm²; secondly, the sign of the chirality of SOT switching reverses at the field of -10 Oe as the magnetization of I-CoFeB is switched, therefore, the effective field from the IEC also reverses the sign. We make the I-CoFeB magnetization along $\pm x$ directions by changing the H_x from ± 100 Oe to 0 Oe, respectively, and the chirality of the field-free SOT switching is clearly reversed for the $\pm x$ I-CoFeB magnetizations due to the opposite effective field from the IEC, as shown in Fig. 2(d).

Then, we change the magnetization of the I-CoFeB layer to the y direction by a magnetic field H_y . In this case the effective field along the y direction from IEC cannot break the inversion symmetry of the P-CoFeB layer (see Supplemental Material [35]). However, the tilted PMA of the P-CoFeB layer from the z axis to the y axis generates a small y -component magnetization of the P-CoFeB layer, as shown in Fig. 3(a); therefore, the inversion symmetry of up and down magnetization states is broken so that the field-free SOT switching can happen. There exists a ferromagnetic IEC between the tilted P-CoFeB and I-CoFeB layers, so the magnetization of the I-CoFeB layer prefers to align along the y axis, which can be seen by the measured small uniaxial magnetic anisotropy along the y axis of the I-CoFeB layer, as shown previously in Fig. 1(b). The Ruderman-Kittel-Kasuya-Yoshida (RKKY) interaction is weak due to the thick (2 nm) space layer of Mo [36], while the magnetostatic coupling

dominates in this system. Most interestingly, when the magnetic field H_y is canted to switch the I-CoFeB layer, the P-CoFeB also switches between the up and down magnetization states due to the IEC. As a result, the AHE signal of the P-CoFeB could be switched by H_y , as shown in Fig. 3(b). The switching field (7.0 Oe) in Fig. 3(b) is smaller than the coercivity (17.0 Oe) of the P-CoFeB layer and agrees with the coercivity (7.0 Oe) of the I-CoFeB along the y axis [Fig. 1(b)], so the possibility of the switching resulting from the misaligned z -component magnetic field could be excluded by this fact. Therefore, when the P-CoFeB layer is switched via SOT, due to the IEC and the very small uniaxial anisotropy of the I-CoFeB, the I-CoFeB layer is also switched at the same time.

Next, we measure the SOT switching under a set of magnetic fields H_y varying from +100 Oe to -100 Oe. As shown in Fig. 3(c), the tilted PMA gives rise to the deterministic SOT switching at zero field, with a switching current density of 2.07×10^7 A/cm². The chirality of SOT switching is the same for ± 5 Oe H_y , while no deterministic SOT switching happens when H_y is larger than ± 10 Oe. This is expected as a larger H_y pins the magnetization of the I-CoFeB layer, and thus the P-CoFeB layer cannot switch individually due to the IEC. We tune the initial I-CoFeB magnetization along $\pm y$ directions by applying the H_y from ± 100 Oe to 0 Oe, respectively, and then measure the field-free SOT switching. We can see that the switching chirality is the same for $\pm y$ initial I-CoFeB magnetizations, as shown in Fig. 3(d), proving that in this case ($\mathbf{J}_e \perp \mathbf{M}$), the zero-field SOT switching comes from the tilted PMA, not the IEC.

Indeed, in the case of $\mathbf{J}_e \perp \mathbf{M}$, apart from SHE, AHE in the I-CoFeB layer could also contribute to the SOT switching. Let us suppose that the spin torque from AHE in the I-CoFeB switches the magnetization of the P-CoFeB, and then the I-CoFeB could also be switched due to the IEC. Since AHE depends on the magnetization of the I-CoFeB, when the I-CoFeB is switched, the spin torque from AHE reverses its sign, which should switch back the magnetization of the P-CoFeB returning to its initial direction. In other words, for the exchange-coupled I-CoFeB/Mo(wedged)/P-CoFeB system, AHE gives no contribution to the deterministic switching.

In order to exclude the SOT from the interlayer Mo, we also measure the SOT switching in the control sample [Mo(2)/P-CoFeB(1.1)/MgO(2)] in addition to the test sample by the same method and with the same +100 Oe H_x . As shown in Fig. 4(a), no SOT switching happens in the control sample, even at a larger current density. This can be attributed to a negligible spin Hall angle of Mo, which agrees with the previous report of the very small spin Hall angle of Mo (0.00023) [37]. By comparing the change of the Hall resistance of SOT-driven and field-driven switching for the test sample, as shown in Fig. 4(a) and 4(b), we can conclude that the SOT switching achieves almost full (94%) switching in this system.

We quantify the SOT efficiency by the current-induced hysteresis loop shift method [13, 38-40]. The damping-like torque of SOT exerts an out-of-plane effective field in the Néel-type domain walls (DWs). As shown in Fig. 5(a), in the absence of an external in-plane magnetic field, the opposite H_z^{eff} in the down-up and up-down DWs gives rise to the same velocity of DW motion, so there is no domain expansion or

shrink; where the interlayer exchange coupling (IEC) and the in-plane field H_x pin the magnetization of the down-up and up-down DWs in the same direction, the same H_z^{eff} in the down-up and up-down DWs could contribute to the domain expansion or shrink, which is reflected from the shift (ΔH_z^{eff}) of R_{xy} - H_z loops.

We can see that the R_{xy} - H_z loops at ± 20 mA are shifted to the opposite field direction even at zero H_x due to the exchange coupling, as shown in Fig. 5(b), which supports the field-free SOT switching. Then we plot the $\chi_{\text{SOT}} = \Delta H_z^{\text{eff}}/J_e$ as a function of the in-plane field H_x , and the saturation value $\chi^{\text{sat}} = -6.02$ Oe/(10^7 A/cm²) is obtained above $H_x = 75$ Oe, where the H_x combined with the exchange coupling overcome the DMI effective field (H_{DMI}). We can further estimate the spin Hall angle of the I-CoFeB: $\theta_{\text{SH}} = (2|e|M_s t_F/\hbar) \times \chi^{\text{sat}} = -0.022$, where the saturation magnetization M_s and the thickness t_F of the P-CoFeB are 1100 emu/cm³ and 1.1 nm respectively, \hbar is the reduced Planck constant, and e is the electron charge.

To date, AHE in ferromagnets has already attracted a great deal of theoretical and experimental attentions for a long time, however, SHE in ferromagnets is ignored. In our work, when there is no AHE contribution in the case of $\mathbf{J}_e // \mathbf{M}$, the observed SOT from the I-CoFeB shows that indeed there is a SHE contribution in ferromagnets. In ferromagnets, compared to AHE-induced spin current, the intrinsic spin current generated by SHE is not subject to dephasing [41], enabling a much longer spin diffusion length. In general, SOC follows the Z^4 (atomic number) dependence, therefore, according to this mechanism, the SOC of CoFeB should be negligible due to the small atomic number. Previous works have also shown that besides of the Z^4

model, the d -orbital filling also plays an important role on SOC [37, 38], and the partially filled $3d$ -orbitals in CoFeB could contribute to the large SOC.

Very recently, a similar work has also reported the field-free SOT switching in the ferromagnet(FM)/Ti/CoFeB trilayer, and they explain it with the interfacial Rashba effect [42, 43] combined with spin precession in the FM/Ti interface [30]. The main argument for their explanation is that this SOT is independent of the magnetization of FM, and this could be understood by considering the bulk SHE in FM. We should point out that their understanding cannot explain our results: firstly, in the I-CoFeB/Mo/P-CoFeB trilayer, Rashba contributions from the bottom I-CoFeB/Mo and top Mo/P-CoFeB interfaces should be cancelled due to the reversed inversion symmetry; secondly, in the case of SOT switching with $\mathbf{J}_e \perp \mathbf{M}$, where \mathbf{M} represents the magnetization of in-plane FM, the generated spin polarization is in colinear with the magnetization direction, therefore, the spin precession process is forbidden due to the relation of $\boldsymbol{\sigma} \times \mathbf{M}$ [44-46].

In conclusion, we have observed the SOT induced magnetization switching in I-CoFeB/Mo(wedged)/P-CoFeB exchange-coupled system, where the SOT comes from a ferromagnetic metal. By tuning the magnetization of the I-CoFeB, two types of field-free SOT switching mechanisms are illustrated: (i) interlayer exchange coupling and (ii) tilted perpendicular magnetic anisotropy. We also show that in both cases, the spin torque comes from the bulk SHE in ferromagnetic metals, while AHE has no contribution. A spin Hall angle $\theta_{SH} = -0.022$ was obtained by the current-induced hysteresis loop shift method, which is comparable with heavy metals such as Pt [47,

48]. This work demonstrates the SOT from a ferromagnetic metal, and the field-free SOT switching opens a door for energy efficient spintronic devices.

Acknowledgements:

This work was partially supported by the NSF Award No. 1611570, Nanosystems Engineering Research Center for Translational Applications of Nanoscale Multiferroic Systems (TANMS), and the Spins and Heat in Nanoscale Electronic Systems (SHINES), an Energy Frontier Research Center funded by the US Department of Energy (DOE), Office of Science, Basic Energy Sciences (BES), under Award No. DE-SC0012670. We are also very grateful to the support from the Function Accelerated nanoMaterial Engineering (FAME) Center and Center for Spintronic Materials, and a Semiconductor Research Corporation (SRC) program sponsored by Microelectronics Advanced Research Corporation (MARCO) and Defense Advanced Research Projects Agency (DARPA).

Figures:

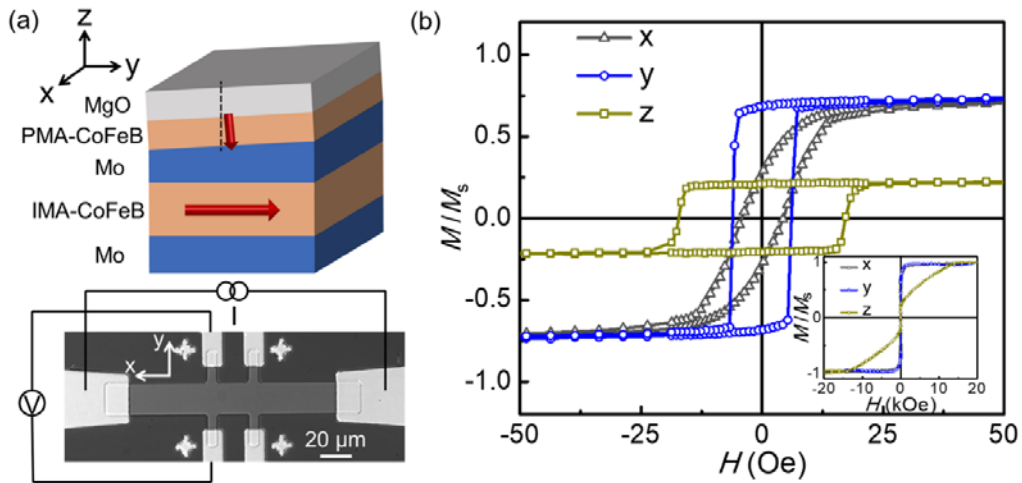


FIG. 1. (a) Schematic of the Mo(2)/I-CoFeB(3)/Mo(2-wedge)/P-CoFeB(1.1)/MgO(2) stack (thickness in nanometers), where the I-CoFeB and P-CoFeB layers have in-plane and perpendicular magnetic anisotropy (IMA and PMA), respectively, and the interlayer Mo is wedged along the y axis. The microscope image in the bottom shows the patterned Hall-bar device, where the current is applied along the x axis. (b) M - H curves under magnetic fields along x , y and z axes, and the inset shows the results at a larger magnetic field range (± 2 T), which clearly shows the IMA of the I-CoFeB layer and the PMA of the P-CoFeB layer, respectively.

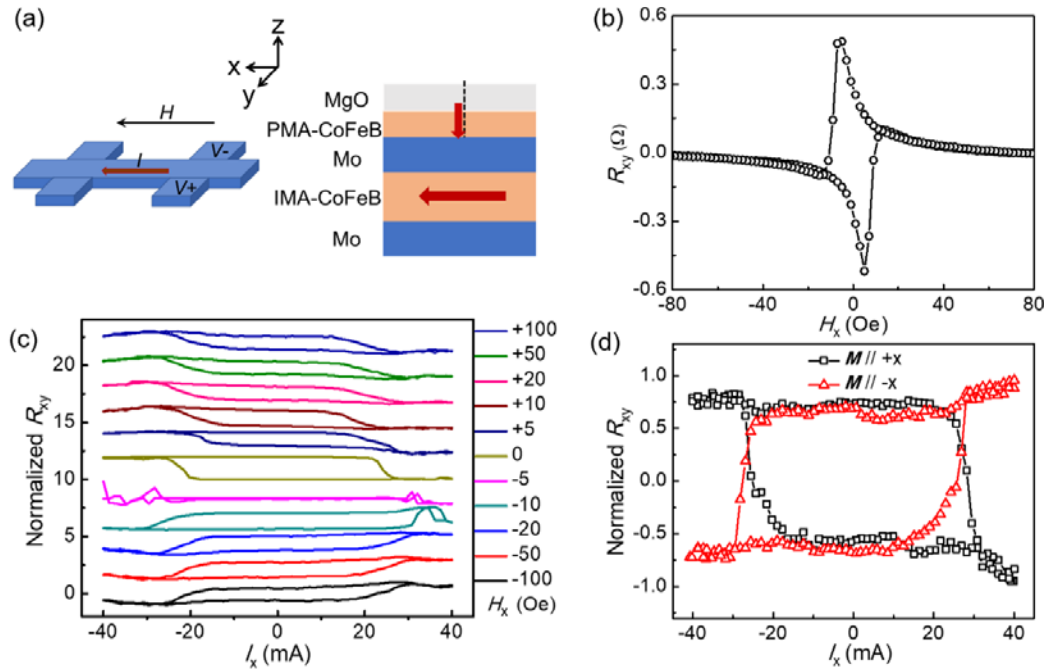


FIG. 2. (a) Schematic of the measurement set up, where the magnetic field is initially applied along the x axis to align the I-CoFeB magnetization; and the cross-sectional view of the film stacks in x - z plane. (b) The planar Hall effect shows the coercivity of I-CoFeB is around 5.5 Oe. (c) SOT induced magnetization switching for varying H_x , a 1-ms writing current pulse I_x is applied to provide SOT to switch the top P-CoFeB layer firstly, and then another 1-ms reading current pulse I_R (1 mA) is applied to read the magnetization of P-CoFeB by AHE resistance, where H_x is varying from +100 Oe to -100 Oe. (d) Field-free SOT switching for $\pm x$ I-CoFeB magnetization directions, respectively, where ± 100 Oe H_x are applied to initialize the I-CoFeB and then removed.

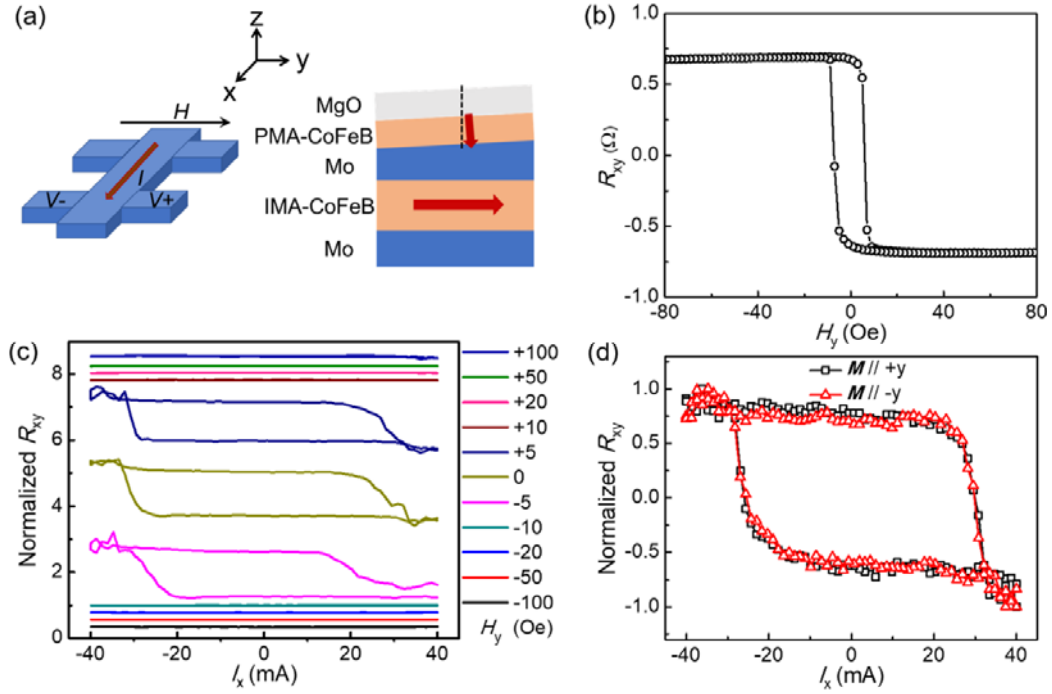


FIG. 3. (a) Schematic of the measurement set up, where the magnetic field is applied along the y axis; and the cross-sectional view of the film stacks in the y - z plane, which shows a wedged Mo interlayer thickness and an induced tilted PMA of the P-CoFeB. (b) As H_y is scanned to switch the I-CoFeB, due to the interlayer exchange coupling, the P-CoFeB also switches between the up and down magnetization states. As a result, the AHE signals can be switched by H_y . (c) SOT induced magnetization switching for a series of H_y , where H_y is varying from +100 Oe to -100 Oe. (d) Field-free SOT switching for the $\pm y$ initial I-CoFeB magnetization directions, respectively.

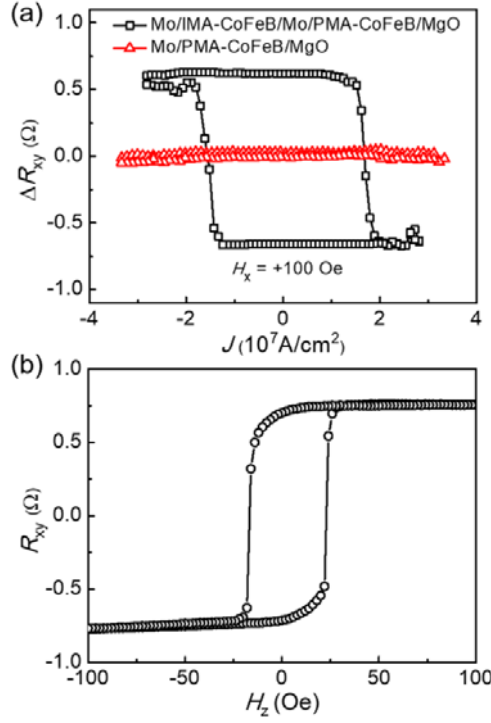


FIG. 4. (a) SOT induced magnetization switching of the control sample [Mo(2)/P-CoFeB(1.1)/MgO(2)] and the test sample [Mo(2)/I-CoFeB(3)/Mo(2-wedge)/P-CoFeB(1.1)/MgO(2)], where a +100 Oe H_x is applied to break the inversion symmetry during the measurement. (b) The R_{xy} - H_z curve of the test sample with a dc current of 1 mA.

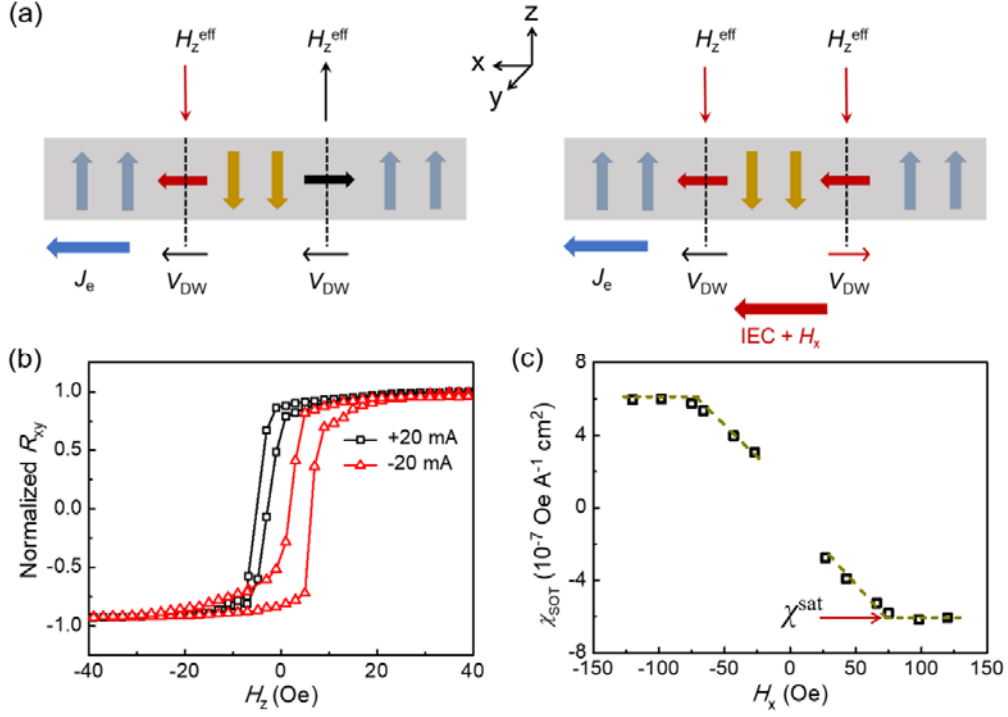


FIG. 5. Current-induced hysteresis loop shift measurement. (a) Schematic of the current-driven domain wall motion, when the interlayer exchange coupling (IEC) and the in-plane field H_x pin the magnetization of the down-up and up-down DWs in the same direction, and thus the domain could expand or shrink. (b) The R_{xy} - H_z curves for ± 20 mA dc current at zero field. The shift of the center field of the hysteresis loop corresponds to the SOT-induced out-of-plane effective field (H_z^{eff}). (c) The extracted χ_{SOT} as a function of H_x , which shows the saturated value of χ_{SOT} .

References:

- [1] I. M. Miron, K. Garello, G. Gaudin, P.-J. Zermatten, M. V. Costache, S. Auffret, S. Bandiera, B. Rodmacq, A. Schuhl and P. Gambardella, *Nature* **476**, 189 (2011).
- [2] L. Liu, C.-F. Pai, Y. Li, H. W. Tseng, D. C. Ralph and R. A. Buhrman, *Science* **336** (6081), 555-558 (2012).
- [3] L. Liu, O. J. Lee, T. J. Gudmundsen, D. C. Ralph and R. A. Buhrman, *Phys. Rev. Lett.* **109** (9), 096602 (2012).
- [4] J. E. Hirsch, *Phys. Rev. Lett.* **83** (9), 1834-1837 (1999).
- [5] S. Zhang, *Phys. Rev. Lett.* **85** (2), 393-396 (2000).
- [6] Y. K. Kato, R. C. Myers, A. C. Gossard and D. D. Awschalom, *Science* **306** (5703), 1910-1913 (2004).
- [7] S. O. Valenzuela and M. Tinkham, *Nature* **442**, 176 (2006).
- [8] J. Sinova, S. O. Valenzuela, J. Wunderlich, C. H. Back and T. Jungwirth, *Rev. Mod. Phys.* **87** (4), 1213-1260 (2015).
- [9] G. Yu, P. Upadhyaya, Y. Fan, J. G. Alzate, W. Jiang, K. L. Wong, S. Takei, S. A. Bender, L.-T. Chang, Y. Jiang, M. Lang, J. Tang, Y. Wang, Y. Tserkovnyak, P. K. Amiri and K. L. Wang, *Nat. Nanotechnol.* **9**, 548 (2014).
- [10] L. You, O. Lee, D. Bhowmik, D. Labanowski, J. Hong, J. Bokor and S. Salahuddin, *P. Natl. Acad. Sci.* **112** (33), 10310-10315 (2015).
- [11] Y.-C. Lau, D. Betto, K. Rode, J. M. D. Coey and P. Stamenov, *Nat. Nanotechnol.* **11**, 758 (2016).
- [12] Y.-W. Oh, S.-h. Chris Baek, Y. M. Kim, H. Y. Lee, K.-D. Lee, C.-G. Yang, E.-S. Park, K.-S. Lee, K.-W. Kim, G. Go, J.-R. Jeong, B.-C. Min, H.-W. Lee, K.-J. Lee and B.-G. Park, *Nat. Nanotechnol.* **11**, 878 (2016).
- [13] S. Fukami, C. Zhang, S. DuttaGupta, A. Kurenkov and H. Ohno, *Nat. Mater.* **15**, 535 (2016).
- [14] W. J. Kong, Y. R. Ji, X. Zhang, H. Wu, Q. T. Zhang, Z. H. Yuan, C. H. Wan, X. F. Han, T. Yu, K. Fukuda, H. Naganuma and M.-J. Tung, *Appl. Phys. Lett.* **109** (13), 132402 (2016).
- [15] S. A. Razavi, D. Wu, G. Yu, Y.-C. Lau, K. L. Wong, W. Zhu, C. He, Z. Zhang, J. M. D. Coey, P. Stamenov, P. Khalili Amiri and K. L. Wang, *Phys. Rev. Appl.* **7** (2), 024023 (2017).
- [16] A. van den Brink, G. Vermeij, A. Solignac, J. Koo, J. T. Kohlhepp, H. J. M. Swagten and B. Koopmans, *Nat. Commun.* **7**, 10854 (2016).
- [17] S. Li, S. Goolaup, J. Kwon, F. Luo, W. Gan and W. S. Lew, *Sci. Rep.* **7** (1), 972 (2017).
- [18] J.-C. Rojas-Sánchez, P. Laczkowski, J. Sampaio, S. Collin, K. Bouzehouane, N. Reyren, H. Jaffrès, A. Mougin and J.-M. George, *Appl. Phys. Lett.* **108** (8), 082406 (2016).
- [19] Y. Fan, P. Upadhyaya, X. Kou, M. Lang, S. Takei, Z. Wang, J. Tang, L. He, L.-T. Chang, M. Montazeri, G. Yu, W. Jiang, T. Nie, R. N. Schwartz, Y. Tserkovnyak and K. L. Wang, *Nat. Mater.* **13**, 699 (2014).
- [20] H. An, Y. Kanno, A. Asami and K. Ando, *Phys. Rev. B* **98** (1), 014401 (2018).
- [21] H. An, T. Ohno, Y. Kanno, Y. Kageyama, Y. Monnai, H. Maki, J. Shi and K. Ando, *Sci. Adv.* **4** (2), eaar2250 (2018).

- [22] T. McGuire and R. Potter, *IEEE Trans. Magn.* **11** (4), 1018-1038 (1975).
- [23] A. A. Kovalev, Y. Tserkovnyak, K. Výborný and J. Sinova, *Phys. Rev. B* **79** (19), 195129 (2009).
- [24] B. F. Miao, S. Y. Huang, D. Qu and C. L. Chien, *Phys. Rev. Lett.* **111** (6), 066602 (2013).
- [25] H. Wu, C. H. Wan, Z. H. Yuan, X. Zhang, J. Jiang, Q. T. Zhang, Z. C. Wen and X. F. Han, *Phys. Rev. B* **92** (5), 054404 (2015).
- [26] S. M. Wu, J. Hoffman, J. E. Pearson and A. Bhattacharya, *Appl. Phys. Lett.* **105** (9), 092409 (2014).
- [27] T. Taniguchi, J. Grollier and M. D. Stiles, *Phys. Rev. Appl.* **3** (4), 044001 (2015).
- [28] Y. Ou, D. C. Ralph and R. A. Buhrman, *Phys. Rev. Lett.* **120** (9), 097203 (2018).
- [29] S. Iihama, T. Taniguchi, K. Yakushiji, A. Fukushima, Y. Shiota, S. Tsunegi, R. Hiramatsu, S. Yuasa, Y. Suzuki and H. Kubota, *Nat. Electron.* **1** (2), 120-123 (2018).
- [30] S.-h. C. Baek, V. P. Amin, Y.-W. Oh, G. Go, S.-J. Lee, G.-H. Lee, K.-J. Kim, M. D. Stiles, B.-G. Park and K.-J. Lee, *Nat. Mater.* **17**, 509 (2018).
- [31] N. Nagaosa, J. Sinova, S. Onoda, A. H. MacDonald and N. P. Ong, *Rev. Mod. Phys.* **82** (2), 1539-1592 (2010).
- [32] K. S. Das, W. Y. Schoemaker, B. J. van Wees and I. J. Vera-Marun, *Phys. Rev. B* **96** (22), 220408 (2017).
- [33] Q. Shao, G. Yu, Y.-W. Lan, Y. Shi, M.-Y. Li, C. Zheng, X. Zhu, L.-J. Li, P. K. Amiri and K. L. Wang, *Nano Lett.* **16** (12), 7514-7520 (2016).
- [34] M. Hayashi, J. Kim, M. Yamanouchi and H. Ohno, *Phys. Rev. B* **89** (14), 144425 (2014).
- [35] See Supplemental Material at [URL will be inserted by publisher] for the SOT switching in the Mo/I-CoFeB/Mo(uniform)/P-CoFeB/MgO structure, the second harmonic Hall measurement, and the robustness test of field-free SOT switching.
- [36] X. Zhang, Y. Zhang and J. W. Cai, *J. Appl. Phys.* **118** (14), 143903 (2015).
- [37] O. Mosendz, J. E. Pearson, F. Y. Fradin, G. E. W. Bauer, S. D. Bader and A. Hoffmann, *Phys. Rev. Lett.* **104** (4), 046601 (2010).
- [38] C.-F. Pai, M. Mann, A. J. Tan and G. S. D. Beach, *Phys. Rev. B* **93** (14), 144409 (2016).
- [39] J. Finley and L. Liu, *Phys. Rev. Appl.* **6** (5), 054001 (2016).
- [40] J. Han, A. Richardella, S. A. Siddiqui, J. Finley, N. Samarth and L. Liu, *Phys. Rev. Lett.* **119** (7), 077702 (2017).
- [41] V. P. Amin, J. Li, M. D. Stiles and P. M. Haney, arXiv:1901.04022 (2019).
- [42] V. P. Amin and M. D. Stiles, *Phys. Rev. B* **94** (10), 104420 (2016).
- [43] V. P. Amin and M. D. Stiles, *Phys. Rev. B* **94** (10), 104419 (2016).
- [44] F. J. Jedema, H. B. Heersche, A. T. Filip, J. J. A. Baselmans and B. J. van Wees, *Nature* **416**, 713 (2002).
- [45] N. Tombros, C. Jozsa, M. Popinciuc, H. T. Jonkman and B. J. van Wees, *Nature* **448**, 571 (2007).
- [46] H. Wu, X. Zhang, C. H. Wan, B. S. Tao, L. Huang, W. J. Kong and X. F. Han, *Phys. Rev. B* **94** (17), 174407 (2016).
- [47] O. Mosendz, V. Vlaminck, J. E. Pearson, F. Y. Fradin, G. E. W. Bauer, S. D. Bader and A. Hoffmann, *Phys. Rev. B* **82** (21), 214403 (2010).
- [48] Z. Feng, J. Hu, L. Sun, B. You, D. Wu, J. Du, W. Zhang, A. Hu, Y. Yang, D. M. Tang, B. S. Zhang and H. F. Ding, *Phys. Rev. B* **85** (21), 214423 (2012).

